

Electrochemically Derived Gradients of the Extracellular Matrix Protein Fibronectin on Gold

Susan T. Plummer, Qian Wang, and Paul W. Bohn*

*Department of Chemistry and Beckman Institute for Advanced Science and Technology,
University of Illinois at Urbana–Champaign, 600 South Mathews Avenue,
Urbana, Illinois 61801*

Rebecca Stockton

*Cardiovascular Research Center, University of Virginia, 415 Lane Road,
Charlottesville, Virginia 22908*

Martin A. Schwartz

*Departments of Microbiology and Biomedical Engineering, Cardiovascular Research Center
and Mellon Prostate Cancer Center, University of Virginia, 415 Lane Road,
Charlottesville, Virginia 22908*

Received February 24, 2003. In Final Form: June 16, 2003

Surface composition gradients of extracellular matrix proteins show great promise as tools in understanding cellular adhesion and motility. The formation of a surface coverage gradient of the protein fibronectin (FN) is described. FN is covalently bound to a counterpropagating two-component gradient formed from thiols with carboxylic acid and hydroxyl terminal functional groups using carbodiimide coupling chemistry. Areas of the surface with initial $-COOH$ termination react with amine groups on the FN, while protein adsorption is resisted on the $-OH$ terminated regions. The $-COOH/-OH$ gradient is generated by applying a linear potential profile to a thin Au gold film on which an 11-mercaptoundecanol (MUD) monolayer is present. A gradient in surface coverage of MUD results, which is then backfilled with 11-mercaptoundecanoic acid (MUA). The $-COOH/-OH$ gradient is characterized by tagging with 200 nm diameter, fluorescently doped, amine-modified nanospheres using the same carbodiimide coupling chemistry and imaging with fluorescence microscopy. The surface coverage of FN on MUA determined by surface plasmon resonance reflectometry is 1.08 ng/mm^2 , with 0.08 ng/mm^2 of physisorbed protein present on MUD. FN gradients are mapped with FTIR external reflection spectroscopy and imaged with fluorescence microscopy by tagging with anti-FN and FITC–IgG. The gradients exhibit a sigmoid shape, with the width of the gradient region occupying $\sim 10\%$ of the total film length. When bovine serum albumin is used to block nonspecific cellular adhesion, the adhesion of the 3T3 fibroblasts to these gradients follows the spatial composition profile of FN.

Introduction

Cell migration is a critical element of immune surveillance, embryonic development, wound healing, and cancer. White blood cells travel through tissue in search of infection, cells in developing embryos move from one site to another, and metastatic cancer cells journey from the initial tumor throughout the body.¹ Cell movement is a highly complex process during which a cell protrudes a region of plasma membrane, which then attaches to the substratum. Using the traction generated by attachment to the substratum, the cell generates mechanical tension to shift its body forward. Adhesions in the back of the cell are released, and the process continues. The detailed molecular steps by which cells migrate are not fully understood.^{2–6} However, it is widely appreciated that

adhesion to proteins in the extracellular matrix (ECM) plays a critical role, including activation of complex intracellular signaling cascades. These pathways ultimately result in actin polymerization and myosin phosphorylation, which in turn drive the mechanical deformations and generate tension.^{7,8} Cells migrate toward gradients of immobilized ECM proteins, a process called haptotaxis.⁴ Haptotaxis is usually examined using modified Boyden chambers in which cells migrate across a porous membrane coated on its lower side by ECM proteins. This system provides readily quantifiable migration but cannot easily be used to observe live, migrating cells. Understanding these complex cell–ECM interactions at the molecular level will be facilitated by ECM model surfaces on which cells can be observed microscopically, and the composition can be controlled from the nanometer to the micrometer length scale.^{9,10} With these model

* To whom correspondence should be addressed. E-mail: bohn@scs.uiuc.edu.

(1) Bray, D. *Cell Movements: From Molecules to Motility*, 2nd ed.; Garland Publishing: New York, 2001.

(2) Horwitz, A. R.; Parsons, J. T. *Science* **1999**, *286*, 1102–1103.

(3) Hynes, R. O. *Trends Biochem. Sci.* **1999**, *24*, M33–M37.

(4) Lauffenburger, D. A.; Horwitz, A. F. *Cell* **1996**, *84*, 359–369.

(5) Webb, D. J.; Parsons, J. T.; Horwitz, A. F. *Nat. Cell Biol.* **2002**, *4*, E97–E100.

(6) Geiger, B.; Bershadsky, A. *Curr. Opin. Cell Biol.* **2001**, *13*, 584–592.

(7) Huttenlocher, A.; Sandborg, R. R.; Horwitz, A. F. *Curr. Opin. Cell Biol.* **1995**, *7*, 697–706.

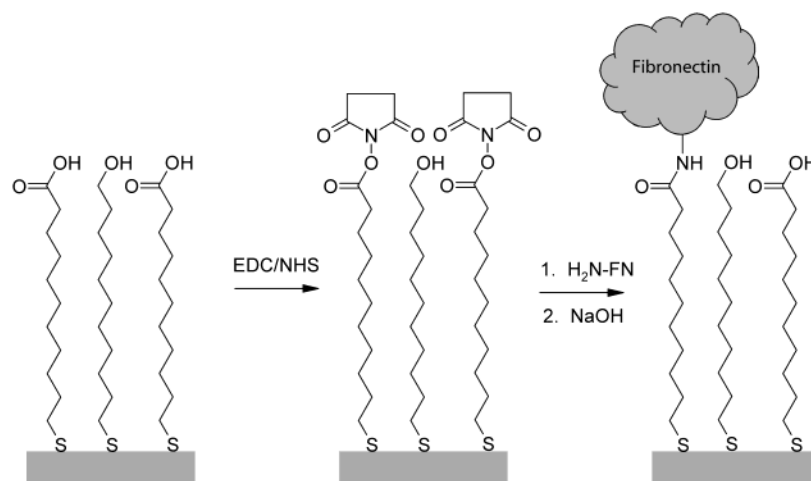
(8) Lauffenburger, D. A. *Nature* **1996**, *383*, 390–391.

(9) Maheshwari, G.; Brown, G.; Lauffenburger, D. A.; Wells, A.; Griffith, L. G. *J. Cell Sci.* **2000**, *113*, 1677–1686.

(10) Bannerjee, P.; Irvine, D. J.; Mayes, A. M.; Griffith, L. G. *J. Biomed. Mater. Res.* **2000**, *50*, 331–339.

(11) Reference deleted.

Scheme 1



surfaces, the cell migration process can be examined in a controlled environment, enabling information on cell morphology, signaling, and function to be integrated with detailed information about the molecular composition of the ECM.

One protein commonly found in the extracellular matrix is fibronectin (FN). FN is a large glycoprotein of MW \approx 450 kDa. It consists of two approximately equal size polypeptide chains attached near the C-terminus by two disulfide linkages. FN contains binding domains for collagen, fibrin, and heparin, as well as several cell-binding sequences.^{12,13} Because of its cell-binding properties, FN is commonly used to study adhesion properties. It has been successfully adsorbed onto various substrates, including tissue culture dishes,^{14–17} optical waveguides,^{18,19} and self-assembled monolayers (SAMs).^{20–24} Once FN is adsorbed, studies of cellular response to the FN-coated substratum are possible.

A drawback of previous adsorption studies is the potential for the exchange of FN with other serum proteins. Albumin, in particular, can readily replace adsorbed FN.¹⁷ To overcome this problem, as well as to control the spatial distribution of FN, this paper reports the covalent attachment of FN to a surface displaying an electrochemically derived composition gradient, using the immobilization chemistry shown in Scheme 1. The covalent binding of FN to a substrate has been demonstrated previously on grafted acrylamide surfaces,²⁵ carboxym-

ethyl-dextran BIAcore chips,²⁶ and other polymer surfaces,^{27,28} but not to SAMs. The strategy employed here is to react free amine groups on FN to an activated succinimidyl ester intermediate, resulting in amide bond formation.^{29,30} Activating agents are *N*-hydroxysuccinimide (NHS) and water-soluble 1-ethyl-3-(3-dimethylaminopropyl)carbodiimide (EDC). This reaction is readily applicable to surface modification of SAMs, as demonstrated by the immobilization of poly(L-lysine),³¹ cytochrome *c*,³² DNA,³³ IgG,³⁴ and other proteins.^{35,36} A variation of this procedure was used previously to immobilize carboxylic acid modified fluorescent polystyrene nanospheres to an amine-terminated SAM in order to characterize the spatial properties of electrochemically derived surface composition gradients.³⁷

Using SAMs as the substrate for FN immobilization has the advantage that the surface functionality presented to the protein for immobilization is highly specific, and the surface can be manipulated to provide spatially varying composition. Surfaces with laterally discontinuous compositions, such as those produced by microcontact printing, have been used to study the growth and adhesion of cells as a function of surface functionality.^{38,39} Surfaces with continuously varying surface functionality hold great

(12) Hynes, R. O. *Fibronectins*; Springer-Verlag: New York, 1990.

(13) McDonagh, J. *Plasma Fibronectin: Structure and Function*; Marcel Dekker: New York, 1985; Vol. 5.

(14) Biran, R.; Webb, K.; Noble, M. D.; Tresco, P. A. *J. Biomed. Mater. Res.* **2001**, *55*, 1–12.

(15) Dimilla, P. A.; Albelda, S. M.; Quinn, J. A. *J. Colloid Interface Sci.* **1992**, *153*, 212–225.

(16) Bentley, K. L.; Klebe, R. J. *J. Biomed. Mater. Res.* **1985**, *19*, 757–769.

(17) Grinnell, F.; Feld, M. K. *J. Biol. Chem.* **1982**, *257*, 4888–4893.

(18) Guemouri, L.; Ogier, J.; Ramsden, J. J. *J. Chem. Phys.* **1998**, *109*, 3265–3268.

(19) Guemouri, L.; Ogier, J.; Zekhnini, Z.; Ramsden, J. J. *J. Chem. Phys.* **2000**, *113*, 8183–8186.

(20) Iuliano, D. J.; Saavedra, S. S.; Truskey, G. A. *J. Biomed. Mater. Res.* **1993**, *27*, 1103–1113.

(21) Mrksich, M.; Chen, C. S.; Xia, Y. N.; Dike, L. E.; Ingber, D. E.; Whitesides, G. M. *Proc. Natl. Acad. Sci. U.S.A.* **1996**, *93*, 10775–10778.

(22) Tidwell, C. D.; Ertel, S. I.; Ratner, B. D.; Tarasevich, B. J.; Atre, S.; Allara, D. L. *Langmuir* **1997**, *13*, 3404–3413.

(23) McClary, K. B.; Ugarova, T.; Grainger, D. W. *J. Biomed. Mater. Res.* **2000**, *50*, 428–439.

(24) Scotchford, C. A.; Gilmore, C. P.; Cooper, E.; Leggett, G. J.; Downes, S. *J. Biomed. Mater. Res.* **2002**, *59*, 84–99.

(25) Verhoeven, M.; Cahalan, P.; Cahalan, L.; Hendriks, M.; Foache, B. In European Patent Application (Medtronic, Inc., USA), Ep, 1994; p 9 pp.

(26) Nakamura, T.; Amano, A.; Nakagawa, I.; Hamada, S. *FEMS Microbiol. Lett.* **1999**, *175*, 267–272.

(27) Nuttelman, C. R.; Mortisen, D. J.; Henry, S. M.; Anseth, K. S. *J. Biomed. Mater. Res.* **2001**, *57*, 217–223.

(28) Webb, K.; Caldwell, K. D.; Tresco, P. A. *J. Biomed. Mater. Res.* **2001**, *54*, 509–518.

(29) Bodanszky, M. *Principles of Peptide Synthesis*; Springer-Verlag: Berlin, 1983; Vol. 16.

(30) Hermanson, G. T. *Bioconjugate Techniques*; Academic Press: New York, 1996.

(31) Frey, B. L.; Corn, R. M. *Anal. Chem.* **1996**, *68*, 3187–3193.

(32) Jiang, L.; Glidle, A.; Griffith, A.; McNeil, C. J.; Cooper, J. M. *Bioelectrochem. Bioenerg.* **1997**, *42*, 15–23.

(33) Pang, D. W.; Zhang, M.; Wang, Z. L.; Qi, Y. P.; Cheng, J. K.; Liu, Z. Y. *J. Electroanal. Chem.* **1996**, *403*, 183–188.

(34) Vaughan, R. D.; O'Sullivan, C. K.; Guilbault, G. G. *Fresenius' J. Anal. Chem.* **1999**, *364*, 54–57.

(35) Patel, N.; Davies, M. C.; Hartshorne, M.; Heaton, R. J.; Roberts, C. J.; Tendler, S. J. B.; Williams, P. M. *Langmuir* **1997**, *13*, 6485–6490.

(36) Lahiri, J.; Isaacs, L.; Tien, J.; Whitesides, G. M. *Anal. Chem.* **1999**, *71*, 777–790.

(37) Plummer, S. T.; Bohn, P. W. *Langmuir* **2002**, *18*, 4142–4149.

(38) Singhvi, R.; Kumar, A.; Lopez, G. P.; Stephanopoulos, G. N.; Wang, D. I.; Whitesides, G. M.; Ingber, D. E. *Science* **1994**, *264*, 696–698.

(39) Whitesides, G. M.; Ostuni, E.; Takayama, S.; Jiang, X. Y.; Ingber, D. E. *Annu. Rev. Biomed. Eng.* **2001**, *3*, 335–373.

promise for the study of cell–ECM interactions. These gradient surfaces have been prepared in a variety of ways, including diffusion,^{40–44} corona discharge,^{45,46} photoimmobilization,^{47,48} microfluidics,^{49,50} and scanning probe microscopy.⁵¹ A technique developed in this laboratory which enables control of surface composition in both space and time (spatiotemporal control) exploits a spatially varying in-plane electrochemical potential to map organothiols onto a surface using their characteristic reductive desorption/oxidative adsorption reactions.^{52,53} This method allows a tunability in gradient properties, such as gradient size and slope, with a greater ease than other preparation methods. When distinct potentials are applied to either end of a thin Au film ($d = 50$ nm), the nonzero resistance of the thin film creates an in-plane surface potential profile given by

$$V(x) = V_0 + \int_0^x \frac{i\rho(l)}{A} dl \quad (1)$$

where V_0 is the offset potential, i is the current, $\rho(l)$ is the position-dependent resistivity, and A is the electrode cross-sectional area. Assuming the position dependence of the resistivity is small, the potential varies linearly as a function of position. Electrochemical reactions may be mapped onto the surface, according to the relative values of the local potential, $V(x)$, and the formal potential for the electrochemical reaction, E^0 . A system that readily lends itself to mapping in this way is the electroadsorption of alkanethiols,^{54–61}



On regions of the electrode surface where the potential is

(40) Elwing, H.; Welin, S.; Askendal, A.; Nilsson, U.; Lundstrom, I. *J. Colloid Interface Sci.* **1987**, *119*, 203–210.

(41) Ruardy, T. G.; Schakenraad, J. M.; vanderMei, H. C.; Busscher, H. J. *Surf. Sci. Rep.* **1997**, *29*, 3–30.

(42) Liedberg, B.; Tengvall, P. *Langmuir* **1995**, *11*, 3821–3827.

(43) Liedberg, B.; Wirde, M.; Tao, Y. T.; Tengvall, P.; Gelius, U. *Langmuir* **1997**, *13*, 5329–5334.

(44) Efimenko, K.; Genzer, J. *Adv. Mater.* **2001**, *13*, 1560.

(45) Lee, J. H.; Kim, H. G.; Khang, G. S.; Lee, H. B.; Jhon, M. S. *J. Colloid Interface Sci.* **1992**, *151*, 563–570.

(46) Lee, J. H.; Lee, J. W.; Khang, G.; Lee, H. B. *Biomaterials* **1997**, *18*, 351–358.

(47) Herbert, C. B.; McLernon, T. L.; Hypolite, C. L.; Adams, D. N.; Pikus, L.; Huang, C. C.; Fields, G. B.; Letourneau, P. C.; Distefano, M. D.; Hu, W. S. *Chem. Biol.* **1997**, *4*, 731–737.

(48) Hypolite, C. L.; McLernon, T. L.; Adams, D. N.; Chapman, K. E.; Herbert, C. B.; Huang, C. C.; Distefano, M. D.; Hu, W. S. *Bioconjugate Chem.* **1997**, *8*, 658–663.

(49) Caelen, I.; Bernard, A.; Juncker, D.; Michel, B.; Heinzelmann, H.; Delamar, E. *Langmuir* **2000**, *16*, 9125–9130.

(50) Jeon, N. L.; Dertinger, S. K. W.; Chiu, D. T.; Choi, I. S.; Stroock, A. D.; Whitesides, G. M. *Langmuir* **2000**, *16*, 8311–8316.

(51) Fuierer, R. R.; Carroll, R. L.; Feldheim, D. L.; Gorman, C. B. *Adv. Mater.* **2002**, *14*, 154–157.

(52) Terrill, R. H.; Balss, K. M.; Zhang, Y. M.; Bohn, P. W. *J. Am. Chem. Soc.* **2000**, *122*, 988–989.

(53) Balss, K. M.; Coleman, B. D.; Lansford, C. H.; Haasch, R. T.; Bohn, P. W. *J. Phys. Chem. B* **2001**, *105*, 8970–8978.

(54) Widrig, C. A.; Chung, C.; Proter, M. D. *J. Electroanal. Chem.* **1991**, *310*, 335–359.

(55) Walczak, M. M.; Popenoe, D. D.; Deinhammer, R. S.; Lamp, B. D.; Chung, C.; Porter, M. D. *Langmuir* **1991**, *7*, 2687–2693.

(56) Weisshaar, D. E.; Lamp, B. D.; Porter, M. D. *J. Am. Chem. Soc.* **1992**, *114*, 5860–5862.

(57) Yang, D.-F.; Wilde, C. P.; Morin, M. *Langmuir* **1996**, *12*, 6570–6577.

(58) Yang, D.-F.; Wilde, C. P.; Morin, M. *Langmuir* **1997**, *13*, 243–249.

(59) Hobara, D.; Miyake, K.; Imabayashi, S.-I.; Niki, K.; Kakiuchi, T. *Langmuir* **1998**, *14*, 3590–3596.

(60) Hatchett, D. W.; Uibel, R. H.; Stevenson, K. J.; Harris, J. M.; White, H. S. *J. Am. Chem. Soc.* **1998**, *120*, 1062–1069.

(61) Stevenson, K. J.; Mitchell, M.; White, H. S. *J. Phys. Chem. B* **1998**, *102*, 1235–1240.

negative of the reductive desorption potential, thiols desorb, while at regions positive of the potential, adsorption is favored, and a transition region of spatially varying composition results between the covered and bare regions. Once a gradient is established by spatially dependent desorption of one thiol, a second thiol component can be backfilled into the bare Au regions, resulting in counter-propagating two-component lateral composition variations. The two components can be chosen to have different ω -termination, thereby creating a surface with spatially varying surface properties. Compared to other methods of creating chemical surface gradients, the electrochemical method used here is distinct in the ease with which the spatial rate of composition may be controlled and also in holding out the possibility of changing the gradient after it has initially been formed. Gradients of various ω -substituted alkanethiols have been generated and characterized using contact angle measurements, surface plasmon resonance imaging, fluorescent labeling with doped polystyrene nanospheres, pulse-force-mode atomic force microscopy, and Raman mapping.^{37,52,53,62,63}

This paper describes the generation of surfaces with gradients in FN coverage, useful in studying the response of cells to varying FN concentrations and observing directed cell growth or migration in the presence of FN concentration gradients. Initially a two-component gradient composed of 11-mercaptoundecanoic acid (MUA) and 11-mercaptoundecanol (MUD) is created. The gradient is characterized by reaction of amine-modified fluorescently doped polystyrene nanospheres to NHS-activated esters of MUA and visualized with fluorescence microscopy. The same coupling procedure is used to react human plasma FN to the gradient surface. Surface plasmon resonance (SPR) reflectometry is used to follow the FN immobilization and tagging, as well as to calculate the resulting FN coverage. The presence of the FN gradient is confirmed with FTIR external reflection spectroscopy by mapping the intensity of the amide I band, present only in the FN complex, across the surface. To image the surface-bound FN with fluorescence microscopy, a two-component sandwich immunoassay is used with anti-FN and FITC–IgG. Finally, the competency of the gradient surfaces to direct the surface adhesion of 3T3 fibroblasts is demonstrated by microscopy.

Experimental Section

Materials. MUA, MUD, and 1-octanethiol (OT) were purchased from Aldrich. EDC, NHS, and goat anti-mouse IgG (whole molecule)–FITC conjugate were purchased from Sigma. Human plasma FN was received either from Gibco-BRL or Sigma. Monoclonal mouse anti-human FN was received either from Chemicon International (clone 3F12) or Sigma (clone FN-15). Red-fluorescent amine-modified FluoSpheres (200 nm diameter) were purchased from Molecular Probes. KOH and NaOH were purchased from Fischer Scientific. All reagents were used as received.

Substrate Preparation. Microscope slides or SF-10 prisms were cleaned in piranha (4:1 H₂SO₄/H₂O₂) cleaning solution. (CAUTION: *Piranha is a vigorous oxidant and should be used with extreme caution.*) An Au film, 50 nm thick, was vapor deposited on the slides as a 10 mm × 3 mm, 6 mm × 1 mm, or 5 cm × 1 cm strip. For the 6 mm × 1 mm strip, thick pads (200–250 nm) separated by 3 mm were deposited over the strip. These pads define an active 3 mm × 1 mm region for gradient formation. An adhesion layer of Cr (1 nm) was deposited under each layer of Au. Samples were stored under N₂ before use. Prior to thiol

(62) Balss, K. M.; Fried, G. A.; Bohn, P. W. *J. Electrochem. Soc.* **2002**, *149*, C450–C455.

(63) Balss, K. M.; Kuo, T.-C.; Bohn, P. W. *J. Phys. Chem. B* **2003**, *107*, 994–1000.

assembly, the films were exposed to O₃ for 30 min, rinsed thoroughly with EtOH, and dried with N₂. O₃ was produced by passing air at a low flow rate by an Hg pen lamp upstream of the sample chamber, so that the sample surface is not exposed to UV radiation. Samples were then immersed in a 1 mM ethanolic solution of thiol for at least 1 h, rinsed with EtOH, and dried with N₂. Substrates for surface plasmon resonance measurements were prepared by evaporating 47 nm of Au with a 1 nm Cr layer directly on an SF-10 prism. Substrates for FTIR measurements have a 5 cm × 1 cm area of 50 nm Au and 1 nm Cr.

Fibronectin Immobilization. Gold films containing a thiol SAM were immersed in a freshly prepared aqueous solution of 75 mM EDC and 15 mM NHS for 15 min. After being rinsed with water, samples were exposed to FN at a concentration of 20 μg/mL in 10 mM phosphate buffer (pH 6.0) for 1 h. The samples were rinsed with water and placed in a Petri dish in 0.1 M NaOH on an orbital shaker at a speed of 40 rpm for 1 h. To characterize the FN layer, samples were exposed to anti-FN (10 μg/mL with 10% goat serum) in pH 6.0 10 mM PB and 100 mM NaCl (PBS) for 1 h and then FITC-conjugated IgG (10 μg/mL with 10% goat serum) in pH 6.0 PBS for 1 h, with water rinses between solutions. Samples were stored in pH 7.4 PBS unless used immediately.

Gradient Formation. Au films with thick connection pads are soaked in 1 mM ethanolic MUD for at least 1 h, rinsed with EtOH, and dried with N₂. Au wire press connections were made to the pads, and the sample was placed in a Teflon electrochemical cell containing an Ag/AgCl reference electrode and a Pt flag counter electrode, with 0.5 M methanolic KOH as the electrolyte. The solution was purged with Ar for 15 min prior to use and during the application of potential. A potential window was applied to the Au film through the wire press connections by a Pine Instruments model AFCBP1 bipotentiostat. The potential window width, ΔV, and the center value of the potential window, V₀, characterized the applied potential window. Potential was applied for 1 min, after which the film was immediately removed from the electrochemical cell and rinsed thoroughly with MeOH and EtOH. The film was immediately placed in a 1 mM ethanolic solution of MUA. After a 1 min assembly time, the sample was rinsed with EtOH and dried with N₂. Samples were stored in water until ready to use, generally within an hour.

Nanosphere Immobilization. Red-fluorescent amine-modified nanospheres (200 nm) were diluted to a concentration of 5.3 × 10⁹ spheres/mL in water. Samples were reacted with 75 mM EDC and 15 mM NHS for 15 min. After being rinsed with water, samples were placed in the nanosphere solution for 30 min. Samples were rinsed with water and EtOH and dried with N₂.

Fluorescence Microscopy. Fluorescence images were collected on a Zeiss Axiovert 100 inverted fluorescence microscope equipped with a Photometrics CoolSnap/ix color CCD camera. To overcome rapid photobleaching, FN samples were mounted with a solution of 0.1% *p*-phenylenediamine, 10% PBS (pH 7.4), and 90% glycerol. Nanosphere images were collected without a mounting solution. Gradient images consist of composite images that have been tiled and aligned using MCID 6.0 software. Intensity values and profiles were also generated using MCID 6.0 software.

Surface Plasmon Resonance Measurements. The apparatus for acquiring SPR measurements has been described previously.⁶⁴ Briefly, an Ar⁺ laser (Coherent Innova 90) pumps a tunable Ti-sapphire laser (TITAN-CW, Schwartz Electrooptics) to produce 752 nm radiation at approximately 100 mW. The light is *p*-polarized by passing through a Soleil-Babinet compensator and line focused onto a Au film (1 nm Cr, 47 nm Au) through an SF-10 prism in the Kretschmann configuration.⁶⁵ A Kel-F flow cell covers the active side of the Au film, with a volume of approximately 150 μL. A Masterflex variable-speed pump with a flow rate range of 0–10 mL/min controls solution flow through the cell. The resonance was monitored in real time by imaging the angular dispersion of the light reflected off the Au film on a CCD camera (Photometrics PM512) using Photometrics CCD9000 software. The resonance curves were fit to a polynomial

from which the angle of minimum reflectance is extracted. Theoretical shifts associated with the adsorption of dielectric layers on the Au surface were calculated using a five-layer Fresnel system. The calibration factor of the SPR system was experimentally determined to be 0.002°/pixel.

FTIR External Reflection Spectroscopy. Fourier transform infrared external reflection (FTIR-ERS) spectra were achieved using a Digilab FTS-60A spectrometer (Bio-Rad, Cambridge, MA) equipped with a Harrick Scientific "Seagull" reflection accessory set to 82° and a liquid nitrogen cooled MCT detector and housed in a N₂-purged glovebox. The experiment was performed with 1024 scans at a resolution of 4 cm⁻¹. All spectra were baseline corrected for accurate interspectrum comparison. Data points were acquired at 5 mm intervals, starting 2.5 mm from the film edge, with a beam size of approximately 2 mm.

Cell Culture and Adhesion Assays. NIH-3T3 cells were cultured in Dulbecco's modified Eagle's medium (DMEM) supplemented with 10% fetal bovine serum, glutamine, penicillin, and streptomycin. For adhesion assays, cells were detached by trypsinization, the trypsin was stopped by addition of soybean trypsin inhibitor, and cells were pelleted by low-speed centrifugation and resuspended in serum-free DMEM. Cell suspensions (2 mL) were added to 35 mm dishes containing FN gradient samples. The gradient samples were blocked with heat-denatured bovine serum albumin (BSA) (95° for 5 min) before exposure to cells. At 1 h, cells were fixed with 3% formaldehyde and rinsed with PBS and images were taken.

Results and Discussion

Fibronectin Reaction. Surface gradients in FN are produced by first forming a surface-confined gradient in a complementary FN-reactive moiety and then mapping FN onto this surface. The reactive component is an activated NHS-ester derived from a thiol-terminated alkanolic acid. The second, non-FN-reactive component of the two-component counterpropagating gradient should ideally resist the adsorption of FN and be unreactive under the conditions used for FN immobilization. Bare Au is not a good option, since FN assembles readily onto that surface.⁶⁶ Surface functionalities which resist protein adsorption, for example, molecules terminating in oligo-(ethylene glycol) moieties, have been identified and would appear to be good candidates for the second component.⁶⁷ In the initial phases of this study, a simple hydroxyl-terminated thiol, MUD, which has also been shown to be effective in reducing protein adsorption, was used.^{68,69} After covalent immobilization of FN onto the activated ester, it is necessary to remove any remaining unreacted FN from the surface, which is accomplished by rinsing the surface with 0.1 M NaOH. The high pH (pH > 12) assists in the hydrolysis of unreacted succinimidyl esters, and the ionic strength reduces electrostatic interactions between FN and the surface, thereby facilitating removal of the physisorbed FN. The NaOH solution is provided either by a constant low-volume flow during SPR experiments or by bathing the sample in the solution under gentle agitation during preparation of gradients for cell assays. In either case, the FN retains its adhesive properties after exposure to NaOH, which is confirmed by its activity in the cell adhesion assay.

Successfully implementing the covalent immobilization of FN requires careful optimization of conditions for each step in the reaction sequence. First is activation of the SAM carboxylic acid groups to enhance their reactivity to

(64) Zhang, Y.; Terrill, R. H.; Bohn, P. W. *Anal. Chem.* **1999**, *71*, 119–125.

(65) Kretschmann, E.; Raether, H. *Z. Naturforsch. A* **1968**, *23*, 2135–2136.

(66) Xiao, C.; Lachance, B.; Sunahara, G.; Luong, J. H. T. *Anal. Chem.* **2002**, *74*, 1333–1339.

(67) Prime, K. L.; Whitesides, G. M. *Science* **1991**, *252*, 1164–1167.

(68) Sigal, G. B.; Mrksich, M.; Whitesides, G. M. *J. Am. Chem. Soc.* **1998**, *120*, 3464–3473.

(69) Ostuni, E.; Chapman, R. G.; Holmlin, R. E.; Takayama, S.; Whitesides, G. M. *Langmuir* **2001**, *17*, 5605–5620.

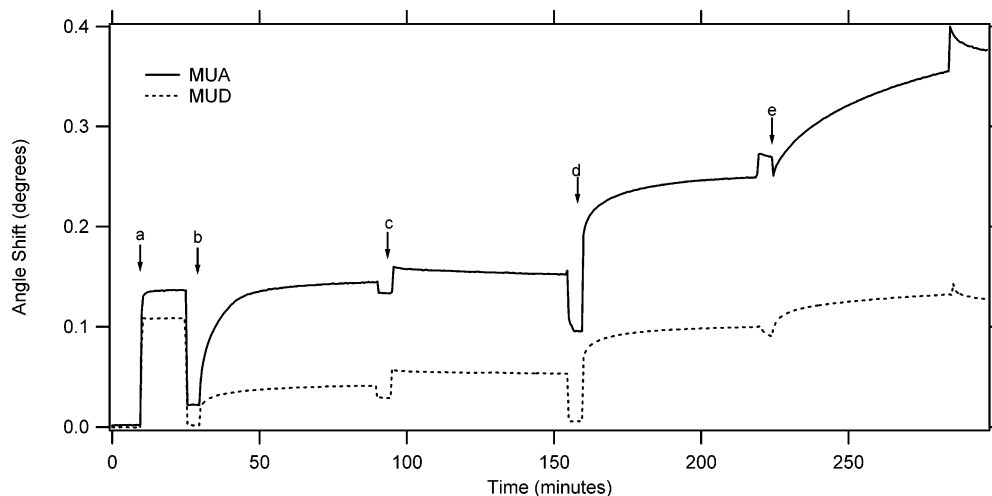


Figure 1. SPR resonance position as a function of reagent exposure/rinsing steps during FN assembly on MUA and MUD. Arrows indicate the introduction of reagents: (a) EDC and NHS, (b) FN, (c) 0.1 M NaOH, (d) anti-FN, and (e) FITC-IgG. Rinse cycles with water were performed at the beginning and end for 10 min each and between reagents for 5 min. The rinse cycle flow rate was 2 mL/min. EDC, NHS, and NaOH cycles had a flow rate of 0.5 mL/min, and the surface was exposed to FN, anti-FN, and FITC-IgG in quiescent solution.

FN. FN contains many exposed and reactive lysine residues. There are most likely multiple bonds formed between the protein and the surface. Lahiri et al. used this active ester reaction scheme with a variety of proteins and determined that optimal reaction occurs at low ionic strength and at a $\text{pH} \sim \text{pI} - 1$.³⁶ While the pI of FN is 5.25 ± 0.25 ,¹² FN aggregates during immobilization at a pH of 4.5, preventing use of the putative optimal pH . At the other extreme, hydrolysis of ester groups occurs at high pH , thus reducing the number of active surface sites. Thus, a pH 6.0 buffer at an intermediate ionic strength of 15 mM was chosen as an effective compromise which minimizes aggregation and hydrolysis simultaneously. After FN is reacted to the ω -succinimidyl ester thiol gradient, a fluorescence sandwich immunoassay is used to view the spatial distribution of FN. Anti-FN is used as a primary tag to recognize the presence of surface-bound FN. After the FN recognition reaction, a secondary FITC-labeled IgG binds to the anti-FN providing visualization through its prosthetic fluorophore.

Optimizing the reaction sequence and quantitatively characterizing the covalently immobilized FN layer are accomplished by monitoring the immobilization with SPR reflectometry. The plasmon resonance of a thin Au film, signaled by a minimum in the reflected light intensity, is sensitive to the dielectric response function of the metal-liquid interface.^{70,71} The angle of minimum reflectance is monitored as a function of time, allowing the assembly of submonolayer films at the Au-electrolyte interface to be monitored in real time. The theoretical position of the resonance minimum (θ_{min}) can be calculated from the Fresnel relations and depends on the dielectric constant of all optical films in the stratified medium as well as the thickness of the surface layers.⁷²

Figure 1 shows the measured shift in θ_{min} ($\Delta\theta_{\text{min}}$) as a function of time for the assembly of FN and tagging reagents on MUA and MUD. To understand how θ_{min} shifts from one reagent to the next, θ_{min} must be compared during exposure to the same solvent superstrate, because there is a non-negligible change in refractive index among different solutions, as evidenced by the $\sim 0.1^\circ$ shift with

the introduction of the EDC and NHS solution. Exposure of the MUA monolayer to EDC and NHS results in a net shift (difference in the ordinate values between points a and b in Figure 1) of 0.022° , a value consistent with that calculated for the formation of succinimidyl esters from MUA. Exposure of the MUD monolayer to the same active ester-forming reagents results in a net shift of 0.002° , which is indistinguishable from the measurement noise. The introduction of FN shows a net $\Delta\theta_{\text{min}}$ (difference in the ordinate values between points b and c in Figure 1) consistent with assembly of a protein film on both MUD and MUA surfaces. The assembly of FN, however, clearly results in a larger shift in θ_{min} on MUA than on MUD, with $\Delta\theta_{\text{MUA}} = 0.112^\circ$ and $\Delta\theta_{\text{MUD}} = 0.027^\circ$. During the NaOH rinse, FN is lost from both monolayers, consistent with the removal of physisorbed FN from both monolayers, as well as the loss of any remaining esters. Following the FN adsorption and NaOH rinse, anti-FN and FITC-labeled IgG are assembled. Both of these solutions have ionic strength $I = 115$ mM, chosen to minimize unwanted nonspecific adsorption. However, it is apparent from the SPR data that some nonspecific adsorption onto the MUD layer does occur. Nonspecific adsorption of the fluorescent IgG species on MUD is low, so it does not interfere significantly with the fluorescence imaging measurements.

Quantitative modeling of the SPR resonance shift data allows the coverage of FN to be calculated, because the magnitude of $\Delta\theta_{\text{min}}$ is dependent upon the dielectric constant and thickness of the adsorbed layer. In this case, the optical response function of the five-layer system composed of prism, Au film, thiol monolayer, FN layer, and water is modeled. In the fitting procedure, the thickness and dielectric constants of the prism, Au film, thiol layer, and water, measured directly or taken from the literature, are held constant, and the composition (and thus the dielectric response) of the FN layer is allowed to vary. Since FN is always present at $<100\%$ monolayer coverage, the FN layer is taken to consist of water and FN, with the thickness of the FN defining the thickness of the layer. The effective dielectric constant of the FN layer is then calculated from the measured $\Delta\theta_{\text{min}}$, assuming a thickness equal to a hypothetical full monolayer of FN. Effective medium theory is used to determine the fractional coverage of FN taking the dielectric constants

(70) Pockrand, I. *Surf. Sci.* **1978**, *71*, 577.

(71) Gordon, J., II *SPIE* **1981**, *276*, 96.

(72) Giergiel, J.; Reed, C.; Ushida, S.; Hemminger, J. *Phys. Rev. B* **1985**, *31*, 3323.

and thicknesses for MUA and MUD layers as $\epsilon_{\text{MUA}} = \epsilon_{\text{MUD}} = 2.10$, $d_{\text{MUA}} = 1.7$ nm, and $d_{\text{MUD}} = 1.6$ nm^{73,74} and those for FN as $\epsilon_{\text{FN}} = 2.25$ and $d_{\text{FN}} = 3$ nm. To determine the coverage of FN, the effective dielectric constant of the 3 nm thick FN layer is back-calculated from the measured $\Delta\theta_{\text{min}}$ after the NaOH rinse (difference in the ordinate values between points a and c in Figure 1). In the assembly sequences shown in Figure 1, $\Delta\theta_{\text{MUD}} = 0.0078^\circ$ and $\Delta\theta_{\text{MUA}} = 0.0938^\circ$ for FN adsorption, corresponding to effective dielectric constants of the FN layers of 1.792 and 1.974, respectively. These effective dielectric constants correspond to $\Gamma_{\text{FN}} = 0.03$ monolayer on MUD and $\Gamma_{\text{FN}} = 0.42$ monolayer on MUA. These coverages can then be related to the mass of FN on the surface using the MW of 450 kDa and specific volume of 964 nm³,⁷⁵ resulting in surface coverages of 0.08 ng/mm² (MUD) and 1.08 ng/mm² (MUA).

Using literature values for the in-plane dimensions of FN of 120 nm \times 3 nm,¹³ the maximum surface coverage of FN is 2.3 ng/mm². Xiao et al. describe the physisorption of FN onto bare Au as monitored with SPR, resulting in a coverage of 3.5 ng/mm²,⁶⁶ a value higher than the close-packed monolayer coverage, indicating that some multilayer formation occurs under conditions relevant to their nonspecifically adsorbed layer. Other studies have looked at the adsorption on polystyrene, showing coverages of 1.9 and 3.2 ng/mm² depending on the surface preparation and adsorption procedure.^{15,76} The coverage of 1.08 ng/mm² obtained from covalent immobilization of FN onto MUA indicates 47% coverage based on molecular dimensions, in good agreement with the 42% coverage calculated based on the specific volume and molecular weight. Thus, there is a high degree of internal consistency between these two measures of the FN coverage on MUA. When FN is assembled onto MUA for 1 h without previously activating the surface with EDC and NHS, an SPR shift of 0.1080° is observed, corresponding to a coverage of 48%, or 1.25 ng/mm². $\Delta\theta_{\text{min}}$ is still increasing after 1 h in this adsorption experiment, indicating that adsorption continues past this time. When the adsorbed FN film is exposed to 0.1 M NaOH for 20 min, 97% of the FN is removed from the surface, suggesting that the adsorbed layer obtained without NHS/EDC is nonspecifically bound and that NHS/EDC activation is required to achieve a significant amount of covalently immobilized FN. Of course, it must be emphasized that the quantitative coverages only have meaning within the context of a given structural model; however, they do provide a good basis for comparison among closely related samples.

Although the foregoing experiments provide a reasonable model for the behavior of FN immobilization at the two single-component ends of a MUD/MUA gradient, a mixture of MUD and MUA resides in the transition region of the gradient. Thus, it is important to understand how the FN immobilization proceeds on mixed MUA/MUD monolayers. To that end, FN has been immobilized on surfaces with varying mixtures of MUA and MUD. As χ_{MUA} increases from 0 to 1, the FN coverage, determined from the SPR resonance shifts, increases approximately linearly ($r = 0.90$). Quantitative fluorescence measurements obtained after performing the sandwich immunoassay on a FN assembly also vary linearly ($r = 0.98$) with χ_{MUA} (Figure 2). In both the SPR and fluorescence

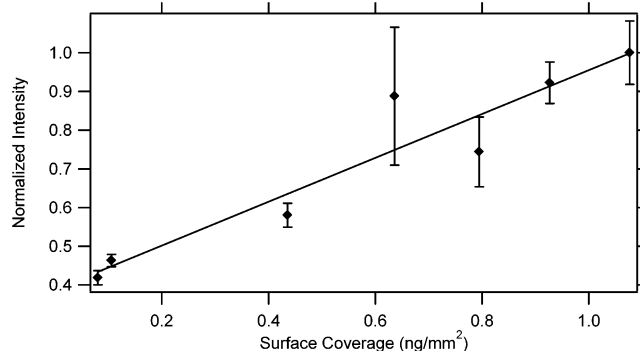


Figure 2. Normalized fluorescence intensity as a function of surface coverage of FN. Surface coverage was determined from SPR resonance shift measurements as detailed in the text. Error bars represent the standard deviation from $n = 3$ samples.

correlations, χ_{MUA} for the monolayer is assumed equal to the solution composition, a reasonable assumption for these two very similar molecules.³⁶ Furthermore, in the calculations for the surface coverage on the mixed monolayers, the SAM thickness was interpolated between the 1.6 and 1.7 nm values appropriate to the two pure components. Finally it should be noted that the FN samples exhibit rapid photobleaching and that consistent quantitative fluorescence measurements require the surface fixing protocol described in the Experimental Section. With these caveats in mind, the correlation between normalized fluorescence intensity and surface coverage shown in Figure 2 can then be used to characterize the FN surface coverage on gradient samples as a function of spatial position.

Gradient Formation. To create FN gradients, a gradient is first formed in MUD and then backfilled with MUA to produce the two-component counterpropagating thiol gradient. Supplying the components in reverse order is also possible, but more consistent results are obtained with the initial gradient formed in MUD. Fluorescent nanospheres have previously been used to image gradients by reacting carboxylic acid modified nanospheres to one-component gradients of 2-aminoethane thiol,³⁷ so the two-component thiol gradients are characterized by reacting fluorescently doped amine-modified polystyrene nanospheres to the gradient in a method analogous to the FN reaction. The nanospheres are 200 nm in diameter and have surface amine functional group loadings of 1.6×10^6 per sphere. After activation of MUA in the gradient with EDC and NHS, the gradient samples are soaked in a 5.3×10^9 mL⁻¹ aqueous solution of nanospheres for 30 min. The solution concentration and reaction time are optimized to maximize reaction to MUA and minimize physisorption onto MUD. Figure 3 shows the fluorescence microscope image of a gradient produced with a potential window of $-500 \text{ mV} \geq E_{\text{appl}} \geq -900 \text{ mV}$ (vs Ag/AgCl reference electrode). From the image, it is clear that the nanospheres react predominantly to the left side, that is, the side associated with the negative end of the potential window, where the initially formed MUD is desorbed and MUA is backfilled. The fluorescence intensity line profile, generated by averaging across the width of the gradient region in steps of 2.56 μm , is shown in Figure 3. The intensity profile is fit to a sigmoid function of the form

$$I(x) = I_b + \frac{I_{\text{max}}}{1 + e^{\{(x_0 - x)/r\}}} \quad (3)$$

where I_b is the baseline intensity, I_{max} is the maximum intensity, x_0 is the inflection point of the slope region, and

(73) Nelson, B. P.; Frutos, A. G.; Brockman, J. M.; Corn, R. M. *Anal. Chem.* **1999**, *71*, 3928–3934.

(74) Frutos, A. G.; Brockman, J. M.; Corn, R. M. *Langmuir* **2000**, *16*, 2192–2197.

(75) Rocco, M.; Infusini, E.; Dega, M. G.; Gogioso, L.; Cuniberti, C. *EMBO J.* **1987**, *6*, 2343–2349.

(76) Grinnell, F.; Feld, M. K. *J. Biomed. Mater. Res.* **1981**, *15*, 363–381.

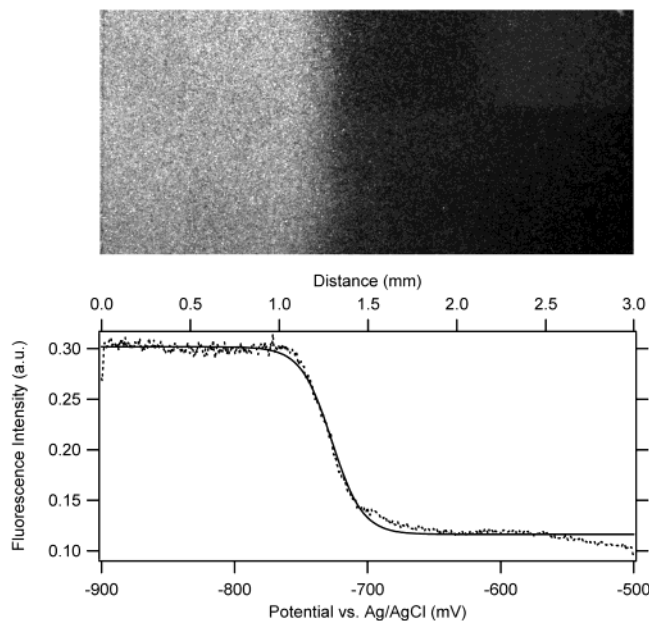


Figure 3. Fluorescence microscope image (top) and spatial intensity profile (bottom) for the immobilization of amine-terminated fluorescent nanospheres onto a MUA/MUD gradient. The intensity profile is shown as a function of both the position across the film and the corresponding surface potential.

r is a constant calculated from the slope. From the fit, the center position, x_0 , and the gradient width, W , defined as the full width at half-maximum of the first derivative of the fit function, dI/dx , are used to characterize the gradient. These parameters can be expressed in either position- or potential-space, assuming a linear potential profile.

Assigning the more negative side of the gradient to $x = 0$, for the gradient in Figure 3, $x_0 = 1.30$ mm and $W = 0.31$ mm. The gradient region therefore occupies ca. 10% of the total length of the Au film, and its center is located slightly to the left of the film center. In potential-space, $x_0 = -727$ mV and $W = 41$ mV. The reductive desorption potential of MUD from Au measured by cyclic voltammetry in the same electrolyte at 100 mV s^{-1} is -975 mV, a value well negative of the observed x_0 . This phenomenon has been observed previously and is attributed to the difference between the temporally varying potential in cyclic voltammetry and the static potential window applied in the gradient formation experiment. These results are consistent with SPR experiments which show desorption of organothiols from Au in static systems to occur at potentials > 100 mV positive of the sweeping desorption potential.^{37,52} The width of the transition region measured by nanosphere fluorescence is somewhat less than the 60 mV width derived from the Fermi–Dirac distribution; however, characterization of two-component gradients by contact angle measurements and atomic force microscopy indicates widths typically greater than 60 mV.^{53,62} The average of 5 samples prepared using the MUD/MUA protocol gives $x_0 = -740$ mV ± 20 mV (1.2 ± 0.1 mm) and $W = 70$ mV ± 20 mV (0.5 ± 0.1 mm), giving an average transition region width of ca. 17% of the film length.

Because FN reacts only with the activated esters derived from MUA, immobilization of FN should follow the spatial distribution of MUA in the gradient structure. The presence of a FN gradient was confirmed with FTIR external reflection spectroscopy and fluorescence microscopy. Figure 4 shows the intensity of the amide I band at 1670 cm^{-1} as a function of position and potential across a 5 cm gradient sample to which FN has been reacted. A fit to the sigmoid function yields $x_0 = -736$ mV (1.99 cm)

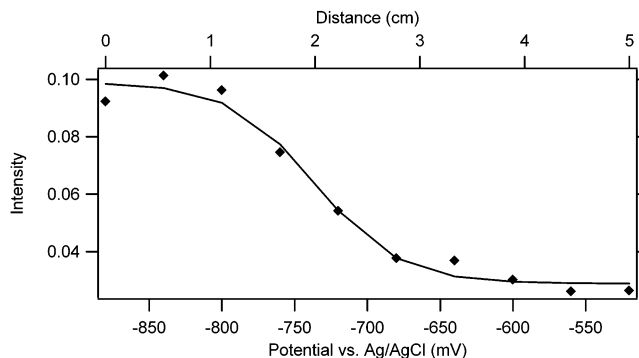


Figure 4. Integrated intensity of the amide I band at 1670 cm^{-1} as a function of position and potential across a 5 cm gradient to which FN has been reacted.

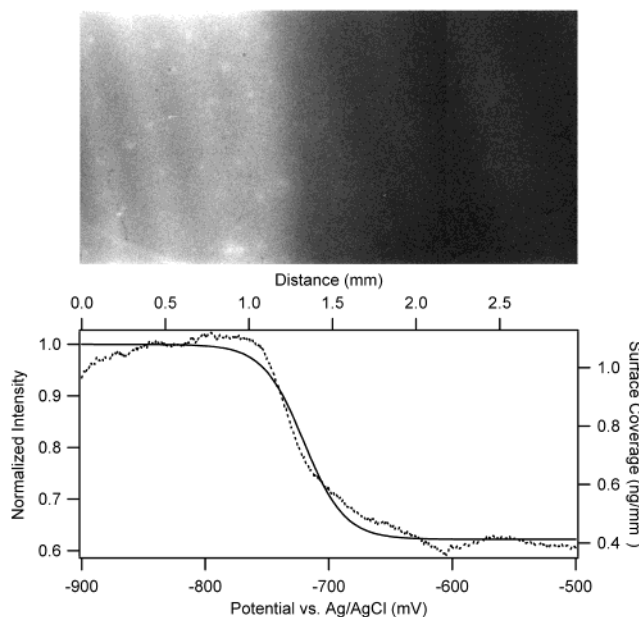


Figure 5. Fluorescence microscope image (top) and spatial distribution of fluorescence intensity and surface coverage (bottom) for an immobilized FN layer gradient on MUA/MUD. The intensity profile and coverage are shown as a function of both the position across the film and the corresponding surface potential. Surface coverage (right ordinate) is obtained from normalized fluorescence intensity and the correlation in Figure 2.

and $W = 102$ mV (1.42 mm). The position of the gradient is approximately the same as that for the nanosphere gradients, but the width is slightly larger. The increase in W is likely a result of spatial averaging due to the large beam area at the grazing angles required in the external reflection measurement. However, the x_0 and W values measured in potential-space on the 5 cm sample by external reflection IR and on the 3 mm sample by nanosphere fluorescence are in reasonable agreement. This consistency in the gradient characteristics, independent of gradient size, is an important feature of this method for producing surface concentration gradients. Gradients ranging from 200 μm to 5 cm in length have now been demonstrated.⁷⁷

Tagging the FN with a sandwich immunoassay of anti-FN and FITC–IgG enables the FN gradient to be viewed directly with fluorescence microscopy. Figure 5 shows the fluorescence microscope image of a gradient with a potential window of -500 mV $\geq E_{app} \geq -900$ mV (vs Ag/

(77) Balss, K. M.; Kuo, T.-C.; Bohn, P. W. *J. Phys. Chem. B*, submitted.

AgCl reference electrode) onto which FN has been immobilized and tagged with anti-FN and FITC-IgG. The normalized intensity profile and sigmoid fitting function are also shown. For this gradient, $x_0 = 1.33$ mm (-720 mV) and $W = 0.43$ mm (58 mV), values which agree well with those seen for the nanosphere-tagged gradients, indicating the presence of buffer during the FN immobilization does not greatly affect the spatial characteristics of the gradient. The surface coverage is then estimated from the normalized intensity using Figure 2. It is important to note that in the mole fraction study of Figure 2, thiols are assembled for 1 h, while in the gradient experiment, the surface is exposed to MUA for only 1 min. The intensity difference between these samples is about 10%, thereby introducing a systematic error into the surface coverage values for the gradient experiments. Furthermore, the surface coverage determined for the MUD side of the gradient is ~ 0.4 ng/mm², higher than the 0.08 ng/mm² coverage seen on the $\chi_{\text{MUA}} = 0$ sample. This fluorescence could be due to physisorbed FN not removed in the NaOH soak or to anti-FN and/or FITC-IgG physisorption onto the surface. Since the surface is only rinsed with water after the tagging procedure, it is likely that some physisorption of the immunoassay reagents occurs.

The advantage of producing gradients in the manner described here is that the position and width of the gradient can be easily manipulated by varying the offset potential and potential window width.³⁷ Figure 6 shows the fluorescence microscope images of a series of gradients in which V_0 has been decreased in steps of 100 mV, with a constant ΔV of 600 mV. The gradients are seen to shift across the film, with $x_0 = 0.72$, 1.19, 1.55, and 2.22 mm, resulting from 600 mV wide potential windows with their negative ends at -900 , -1000 , -1100 , and -1200 mV versus Ag/AgCl, respectively. The widths of the gradients also vary, with $W = 0.14$, 0.27, 0.35, and 0.36 mm, respectively. The variation in W as a function of x_0 has been described previously and is thought to be related to thiol desorption kinetics.³⁷ As with the gradient in Figure 5, the surface coverage on the MUD side of the gradient has a higher coverage than the 0.08 ng/mm² seen for $\chi_{\text{MUA}} = 0$ in Figure 2.

Cellular Adhesion. The purpose of producing FN gradients is to study the effect of FN concentration on cell adhesion, spreading, and motility. To verify that the gradients described in this paper will serve that purpose, NIH-3T3 fibroblast cells were plated onto a MUA/MUD-derived FN gradient surface that was pretreated with denatured BSA. The BSA serves to block the surface underneath the FN, thereby preventing adsorption of cell-derived FN or other adhesive proteins. This block is necessitated by the nonspecific adhesion of cells onto the MUD surface. The adhesion of cells on the FN/BSA gradient is shown in Figure 7. The cells adhere and spread on the FN side of the gradient, no cells are present on the MUD side, and a clear transition is seen between regions that promote and hinder adhesion. The adhesion of cells on the gradient clearly follows the pattern established by the FN gradient.

Conclusion

The spatiotemporal control of surface composition afforded by the in-plane control of electrochemical potential distributions is extended to the creation of surfaces having a well-defined gradient in the surface concentration of covalently immobilized FN. An effective strategy involves creating a counterpropagating two-component

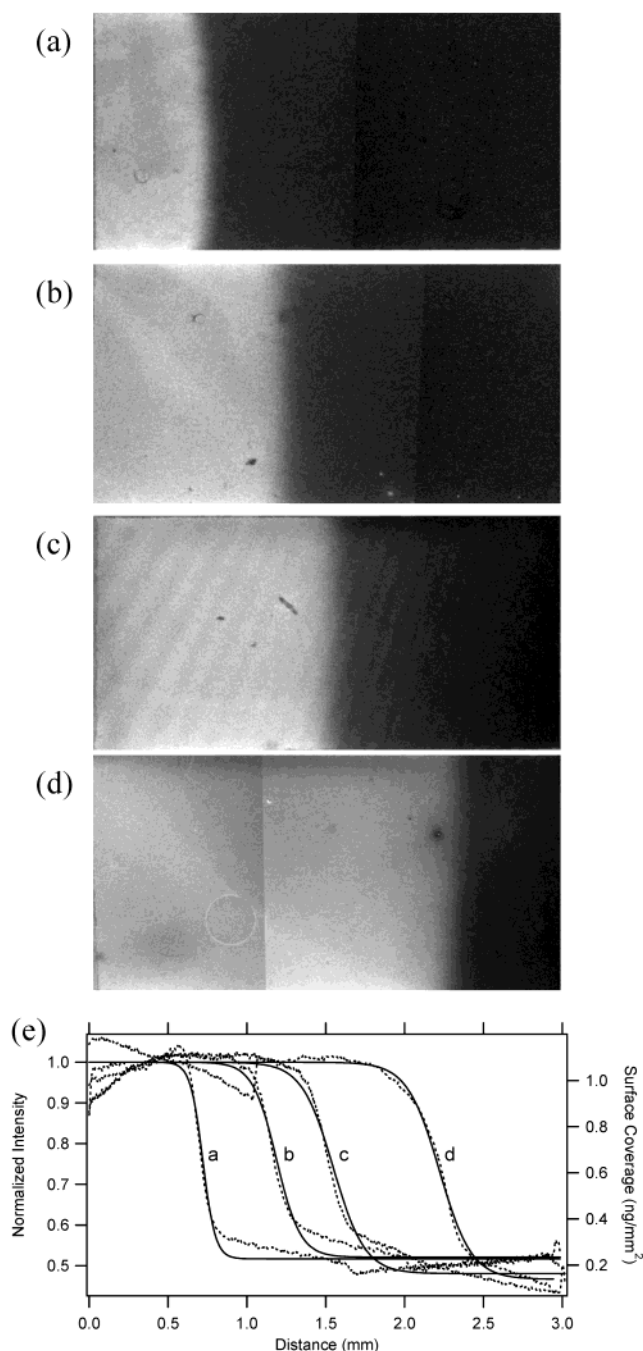


Figure 6. Fluorescence microscope images of FN gradients prepared on gradients with potential windows of (a) -300 to -900 mV, (b) -400 to -1000 mV, (c), -500 to -1100 mV, and (d) -600 to -1200 mV vs Ag/AgCl. (e) Spatial fluorescence intensity and surface coverage as a function of position for the FN gradients prepared in (a)–(d).

gradient from precursor organothiols, one of which can be selectively activated toward reaction with pendant primary amine functionalities on the protein. The other component is chosen to be unreactive toward FN immobilization and to be inherently resistant to protein adhesion. Activation of surface-bound MUA in MUA/MUD gradients through a water-soluble carbodiimide and *N*-hydroxysuccinimide followed by reaction with FN results in surfaces on which the FN spatial distribution mimics that of the MUA precursor. Reaction of FN to a two-component MUD/MUA gradient results in the formation of a gradient in FN concentration between 1 ng/mm² on the MUA end and 0.2 ng/mm² on the MUD end. The transition region of the gradient shows a sigmoid variation

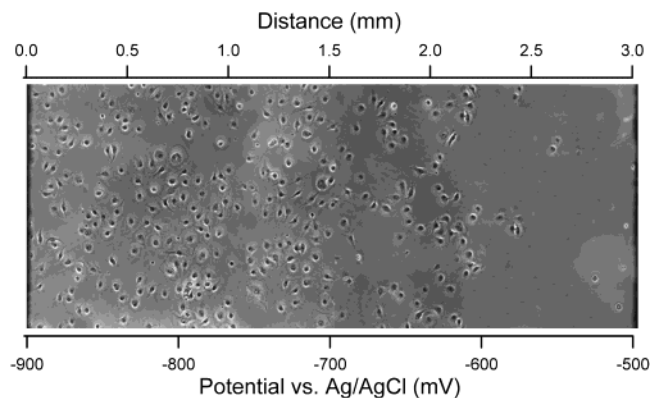


Figure 7. Optical micrograph showing the adhesion of 3T3 fibroblast cells on a MUA/MUD-derived FN/BSA gradient. The top and bottom *x*-axes give the spatial/potential distribution of adhesion.

in the FN coverage, typically encompassing 10–20% of the total sample width. It is anticipated that the gradient

slope in the transition region, a critical parameter for quantitative studies of cell adhesion and motility, can be readily controlled through the width of the applied potential window in physical space and by control of the areal density of reactive esters derived from MUA. These FN gradients are competent for studies of cell adhesion and motility, as demonstrated by the selective adhesion of 3T3 fibroblasts on the FN regions. The process by which the gradient is formed is not specific to FN, requiring only the presence of solvent-accessible primary amines, thus lending itself readily to the immobilization of a variety of other biological macromolecules of interest.

Acknowledgment. The work reported here was supported by the National Science Foundation through Grant CHE99-10236 and by the National Institute of General Medical Sciences through the Cell Migration Consortium, GC10825.

LA030075R